

Electronic structure of CrO₂ as deduced from its magneto-optical Kerr spectra

J. Kuneš and P. Novák

Institute of Physics, Academy of Sciences, Cukrovarnická 10, CZ-162 53 Prague, Czech Republic

P. M. Oppeneer

Institute of Solid State and Materials Research, P.O. Box 270016, D-01171 Dresden, Germany

C. König, M. Fraune, U. Rüdiger, and G. Güntherodt

II. Physikalisches Institut, RWTH Aachen, D-52062 Aachen, Germany

C. Ambrosch-Draxl

Institut für Theoretische Physik, Universitätsplatz 5, Universität Graz, A-8010 Graz, Austria

(Received 6 August 2001; published 4 April 2002)

We report a combined experimental-computational investigation of the electronic structure of CrO₂. We have measured the magneto-optical Kerr spectra of CrO₂ at 10 K and 300 K. At 10 K the Kerr signal is significantly enhanced over that obtained at 300 K. We compare the measured Kerr spectra to first-principles theoretical spectra, which we computed using three different approximations to the exchange-correlation functional, i.e., the local spin-density approximation (LSDA), generalized gradient approximation (GGA), and LSDA+*U*. The experimental low-temperature magneto-optical Kerr spectra are best explained by calculations employing the GGA functional. The addition of an on-site Coulomb correlation *U* does not lead to reasonable Kerr spectra.

DOI: 10.1103/PhysRevB.65.165105

PACS number(s): 78.20.-e, 71.20.-b, 71.28.+d

I. INTRODUCTION

CrO₂ has recently attracted attention because of its unusual electronic structure and magnetic properties.¹⁻⁹ CrO₂ is a ferromagnetic conductor in the group of mostly antiferromagnetic insulating 3*d* transitional-metal oxides. Moreover, *ab initio* investigations predicted its electronic structure to be anomalous,¹ with only electrons of majority-spin polarization appearing at the Fermi level resulting in so-called “half-metallic” behavior. The half-metallic property has important applications in devices based on tunneling magneto-resistance^{10,11} and intergrain-tunneling magneto-resistance.^{4,12-14}

The most interesting and controversial issue is, from a fundamental point of view, the role of the on-site Coulomb correlation. Already the first *ab initio* calculation¹ based on the local spin-density approximation (LSDA) predicted correctly the metallic ground state of CrO₂. In spite of this, the LSDA approach is well known to fail to predict the proper electronic structure of most of the other 3*d* metal oxides. The inclusion of the gradient corrections to the LSDA (generalized gradient approximation, or GGA) does not normally improve the electronic structure description of the 3*d* metal oxides. The reason for this failure of the LSDA and GGA functionals is the insufficient treatment of the on-site Coulomb correlation. In this respect, the LSDA+*U* method,¹⁵ which includes explicitly an on-site correlation term, has brought an important improvement to the description of most 3*d* metal oxides, because it correctly yields the insulating ground state. Also spectral properties of transition-metal oxides are better described by the LSDA+*U* method.^{15,16} In the case of CrO₂ the question has risen as to whether the LSDA+*U* method also correctly yields its electronic struc-

ture. Arguments supporting positive¹⁷ as well as negative¹⁸ answers have been published.

In the present work we address this question from the point of view of the magneto-optical spectra of CrO₂, which depend sensitively on the electronic structure. We report here polar Kerr rotation and ellipticity spectra that were measured on epitaxially grown, *a*-axis textured CrO₂ films in the range from 1.2 to 4.9 eV at 10 K and 300 K. These experimental spectra are compared to theoretical spectra which we computed using either the LSDA, GGA, or LSDA+*U* exchange-correlation functionals. Furthermore, a detailed analysis of the contributing optical transitions is performed, and the anisotropy of the Kerr effect is studied. In some respects this paper extends the previous investigations of the optical spectra, calculated by Brändle *et al.* (Ref. 19) and by Mazin *et al.* (Ref. 18), to the case of magneto-optical effects studied by Uspenskii *et al.* (Ref. 20). The most important topic, however, is the comparison of the LSDA, GGA, and LSDA+*U* approaches, which, to our best knowledge, has not been presented so far. On the basis of that comparison we conclude that the experimental magneto-optical Kerr spectra of CrO₂ are best explained by calculations based on the GGA functional. As a consequence, the electronic structure of CrO₂ is reasonably well described by the GGA functional, without the need to invoke an additional on-site Coulomb *U* correlation.

II. EXPERIMENT

The CrO₂ films were prepared by a chemical vapor deposition process proposed by Ishibashi *et al.* (Ref. 21). Al₂O₃ (0001) substrates were annealed at 1000 °C for several hours before starting the deposition process. During the deposition the substrate is oriented at an angle of 30° with respect to the

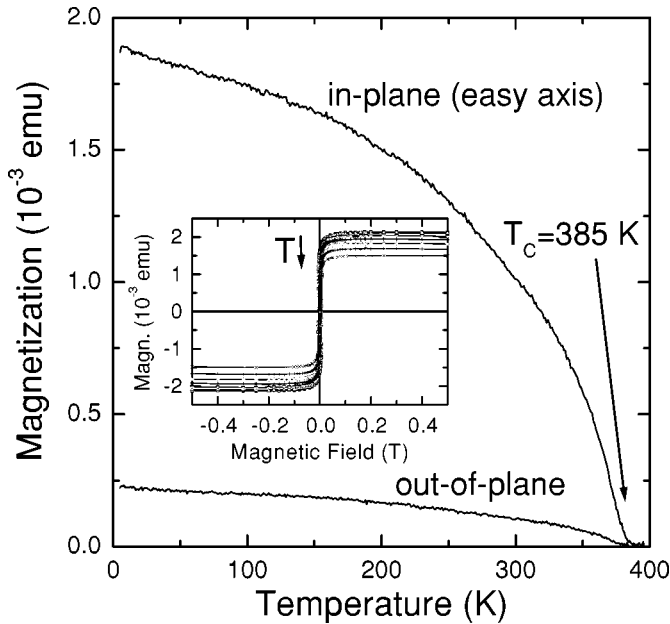


FIG. 1. Temperature dependence of the remanent magnetization of an a -axis-oriented CrO_2 film in in-plane and out-of-plane geometries after saturating with an in-plane field. The inset shows hysteresis loop measurements with the in-plane field at 10, 25, 50, 100, 150, 200, 250, and 295 K.

horizontal axis of a tube furnace. CrO_3 is evaporated at 260°C within a two-zone tube furnace. A well-controlled oxygen flow transports the evaporated material and its intermediate oxide phases to the deposition zone where the substrate is placed. The substrate temperature is adjusted to 390°C enabling the growth of CrO_2 . According to the phase diagram, CrO_3 reduces via several chromium oxide states to CrO_2 (Ref. 22). The growth of a 200 nm thick CrO_2 film takes several hours. Using Al_2O_3 (0001) substrates a columnar growth of a -axis-oriented CrO_2 on an initial Cr_2O_3 layer has been found in transmission electron microscopy as well as in x-ray-diffraction investigations. The sixfold in-plane symmetry of the (0001)-oriented Cr_2O_3 initial layer leads to three equivalent in-plane orientations for the $\{001\}$ plane of the CrO_2 unit cell as confirmed by electron diffraction and scanning electron microscopy. A detailed structural and magnetotransport characterization of these films will be published elsewhere.²³

The ferromagnetic ordering temperature of CrO_2 is in the range of 385–395 K (Refs. 22 and 24). The measured temperature dependence of the magnetization, see Fig. 1, shows a significant reduction of the saturation magnetization at room temperature. Room temperature is already close to the T_C of CrO_2 , so that a magnetization reduction is expected. The temperature dependence of the magnetization was measured using the Kerr effect, wherefore the magnetization can be somewhat less than that of a superconducting quantum interference device measurement. The room-temperature magnetization reduction motivated the current low-temperature polar Kerr spectroscopy measurements. Previous polar Kerr spectra of CrO_2 were measured only at room temperature.²⁵ The inset shows in-plane hysteresis loops at

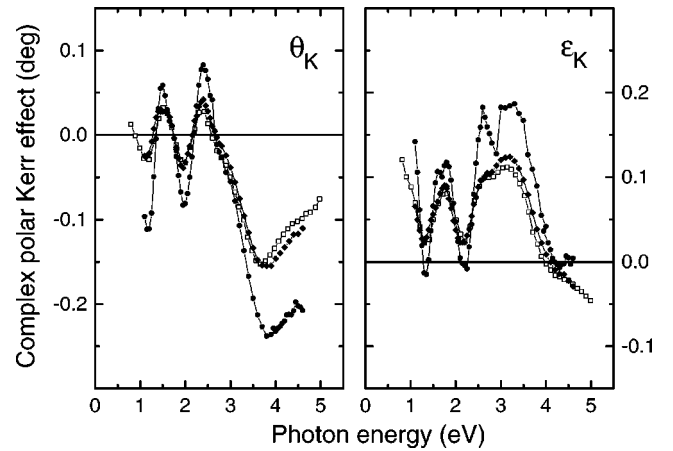


FIG. 2. The polar Kerr rotation θ_K and Kerr ellipticity ε_K of CrO_2 measured at two different temperatures. Closed symbols: this work, for 10 K (\bullet), and 300 K (\blacklozenge). Open symbols: the room-temperature results of Brändle *et al.* (Ref. 25).

temperatures of 10, 25, 50, 100, 150, 200, 250, and 295 K which indicate an in-plane easy magnetization axis over the whole temperature range investigated.

A fully automated polar Kerr spectrometer was used to measure the polar Kerr rotation and ellipticity spectra in the photon energy range from 1.2 to 4.9 eV. An optical cryostat inset allowed measurements from 10 K to room temperature. All data were recorded relative to an Al mirror. During the measurements, the CrO_2 films were magnetized with an out-of-plane field of $B = \pm 1.5$ T to reduce birefringence effects. In Fig. 2 we show the present low-temperature and room-temperature Kerr spectra measured on the prepared films, as well as those measured at 300 K by Brändle *et al.* (Ref. 25). There exists a pronounced effect of temperature on the small structures in the Kerr rotation below 3 eV. The (negative) Kerr rotation peak at 1.2 eV is almost four times larger at 10 K. Also the other small Kerr rotation peaks at 1.5, 2.0, and 2.4 eV become two times larger. Our measured Kerr spectra are apparently consistent with the previous room-temperature spectra.²⁵ In the low-temperature Kerr ellipticity there occurs a sudden dip at 2.8 eV, which is not present in the room-temperature spectrum. It could be that this feature is an experimental artifact. In view of the considerable influence of temperature on the Kerr spectra, our low-temperature data are the optimal starting point for performing a critical comparison to *ab initio* calculated Kerr spectra.

III. POLAR KERR EFFECT IN BIAxIAL CRYSTALS

The measurements are performed on CrO_2 films where the tetragonal c axis of the rutile structure is in the film plane, and one of the a axes is perpendicular to the film. This setup does not correspond to the standard situation of a uniaxial crystal, commonly treated in the literature. In the case of normal incidence the polarization analysis of the polar Kerr effect reduces to a two-dimensional problem in the plane normal to the propagation of the light. For a uniaxial crystal, where the magnetization is oriented along an axis of at least threefold symmetry, the two diagonal elements of the

dielectric tensor corresponding to the axes perpendicular to the magnetization are equal. This facilitates the polarization analysis considerably. In the present situation, however, these two diagonal elements are unequal. The problem of the two diagonal elements of the dielectric tensor being different was studied by Uspenskii *et al.* (Ref. 20). Since this arrangement is not very common we discuss it in more detail.

Unlike the uniaxial case, where only magnetic circular dichroism is present resulting from breaking of the time-inversion symmetry, an additional nonmagnetic linear dichroism that arises from the low real-space symmetry appears in the studied case. The nonmagnetic part of the rotation and ellipticity depends on the orientation of the polarization vector of the incident light with respect to the crystal axes. The magnetic part of the rotation and ellipticity changes sign under reversal of magnetization, while the nonmagnetic part remains unchanged. In the following the axes of the dielectric tensor are chosen to coincide with the crystallographic axes such that x is along the tetragonal c axis, and the magnetization and one a axis are along z . Starting from the assumption that the nonmagnetic effect characterized by $\sigma_{xx}-\sigma_{yy}$ is much larger than the magnetic one characterized by σ_{xy} , we derived an expression for the magnetic part of the rotation and ellipticity, i.e., the Kerr rotation θ_K and ellipticity ε_K (see the Appendix). An additional assumption that both the magnetic and nonmagnetic rotations are smaller than a few degrees was used. When we define θ_K and ε_K as half of the difference between the rotations and ellipticities, respectively, obtained for opposite orientations of the magnetization, we obtain

$$\theta_K + i\varepsilon_K = \epsilon_{xy} \left(\frac{r_y - r_x}{\epsilon_{yy} - \epsilon_{xx}} \right) \frac{r_x \cos^2 \phi + r_y \sin^2 \phi}{r_x^2 \cos^2 \phi + r_y^2 \sin^2 \phi}. \quad (1)$$

Here $\epsilon_{\alpha\beta}$ are elements of the permittivity tensor and ϕ is the angle between the polarization vector of the incident light and the y axis. The reflection coefficients r_x and r_y are given by

$$r_\alpha = \frac{\sqrt{\epsilon_{\alpha\alpha} - 1}}{\sqrt{\epsilon_{\alpha\alpha} + 1}}. \quad (2)$$

The in-plane distribution of crystallites in the studied film approximately corresponds to a random ϕ . Averaging expression (1) over ϕ one arrives at

$$\theta_K + i\varepsilon_K = \frac{2\epsilon_{xy}}{\epsilon_{yy} - \epsilon_{xx}} \frac{r_y - r_x}{r_y + r_x}. \quad (3)$$

We note that formula (1) differs from the expression given by Uspenskii *et al.* (Ref. 20). While the two expressions are identical in the limiting cases $\phi=0, \pi/2$, the dependence on ϕ is different. We analyzed this discrepancy and found that it comes from a different application of the approximation, which is that the nonmagnetic rotation is small. When that condition is fulfilled both formulas give practically the same results.

IV. COMPUTATIONAL METHOD

We have used the full-potential linearized augmented plane-wave method as implemented in the WIEN97 code²⁶ in the present work. The exchange field, whose orientation is treated as an external parameter, is assumed to be collinear in all points in space. The spin-orbit coupling is included within the second variational approach.²⁷

The calculations were done in two steps. First the electronic structure was converged to self-consistency and then the optical and magneto-optical spectra were computed. The linearized augmented plane-wave basis, characterized by the muffin-tin-sphere radii of 1.95 a.u. (1.6 a.u.) for chromium (oxygen), consisted of approximately 820 functions, while the oxygen $2s$ and chromium $3s$ and $3p$ semicore states were treated as local orbitals. A regular sampling of the Brillouin zone (BZ) with 3380 k points was used in the iterative computation of the electronic structure, whose amount was increased to 7514 k points in the BZ for the calculation of the optical and magneto-optical properties. The irreducible k points were determined out of these samplings in accordance with the actual symmetry that depends on the exchange-field direction. Linear-response formalism was employed to compute the optical conductivity or dielectric tensor within the dipolar approximation (for details, see Refs. 28 and 29). The absorptive part of the components of the dielectric tensor was calculated up to 2 Ry, providing a sufficiently large energy interval for the Kramers-Kronig transformation and the determination of the refractive part up to 8 eV.

The whole computational procedure was repeated six times. The (001) and (100) orientations of the exchange field were studied, each for three different exchange-correlation functionals, viz., the LSDA (Ref. 30), GGA (Ref. 31), and LSDA+ U (Ref. 32). An extra calculation was performed with the GGA functional for the (011) exchange-field orientation.

We employed for the LSDA+ U approach the rotationally invariant formulation³³ with the ‘‘double-counting’’ term of Anisimov *et al.* (Ref. 16). The theoretical U and J parameters of Korotin *et al.* (Ref. 17) were used.

V. RESULTS

A. Bonding and partial densities of states

CrO₂ crystallizes in the rutile structure which is built of O octahedra surrounding the Cr atoms that form a body-centered tetragonal lattice. It has become customary to introduce a local coordinate system according to the Cr-O bonding axes within the octahedra.^{17,34–36} The octahedra that surround the corner and the body-centered Cr site are rotated by 90° along the c axis with respect to one another, whereas the apex axes of each of the octahedra are oriented perpendicular to the crystallographic c axis. The octahedra are slightly irregular with a rectangular base, whose longer side is parallel to the c axis. The Cr-O distance within the base is 1.8% longer than the one in the perpendicular direction, which we denote as the local Z direction. This defines a

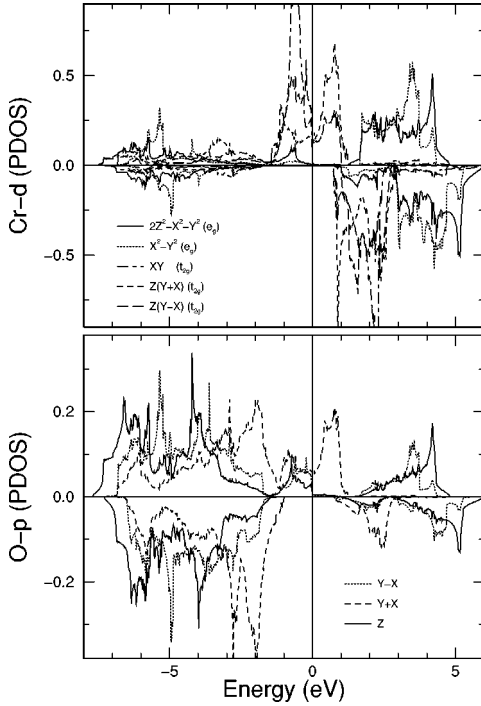


FIG. 3. Partial Cr-*d* (upper panel) and O-*p* (lower panel) densities of states of CrO₂ as calculated with the GGA. Negative values correspond to the minority-spin polarization.

natural local coordinate system at the Cr site, such that the *X* and *Y* axes point approximately to the O sites, and, in particular, *Y-X* is parallel to the longer base side. The natural coordinates are denoted by capital letters *X*, *Y*, and *Z* to avoid confusion with the global coordinates *x*, *y*, and *z*.

The bonding, which concerns only Cr-*d* and O-*p* states, has been discussed by several authors.^{1,18,34,35,37} As the partial densities of states (PDOS) were previously reported for the LSDA and LSDA+*U* exchange-correlation functionals, we present here only the PDOS obtained with the GGA functional. In Fig. 3 we show the GGA-derived Cr-*d* and O-*p* partial densities of states. A well-developed splitting of the Cr-*d* states by the quasicubic crystal field is obtained. The position of the *e_g* orbitals, which point to the O sites, is responsible for the higher-energy PDOS, which in turn is due to the Coulomb repulsion by the *p* charge. The position of the *e_g* orbitals towards the O sites is also responsible for the larger degree of *p-d* hybridization as compared to the *t_{2g}* orbitals, whose lobes point to the space in between the O sites. The *p-d*(*e_g*) hybridization is reflected by the *d*(*e_g*) peaks at the top of the *e_g* antibonding band and at the bottom of the *p* bonding band; corresponding *p* peaks can be observed as well. The contraction of the Cr-O distance along the local *Z* axis is reflected in the $(2Z^2 - X^2 - Y^2)$ peak shifted above the corresponding $(X^2 - Y^2)$ peak. As the *p*(*Y+X*) position is perpendicular to the plane of adjacent Cr atoms, no hybridization with *d*(*e_g*) states is found. The present PDOS study, as well as previous studies,^{34,35} support for CrO₂ the picture of ionic bonding with additional Cr-*d*-O-*p* hybridization. Together with the strong exchange interaction at the Cr sites, this bonding gives rise to the half-metallic nature^{5,9} of CrO₂.

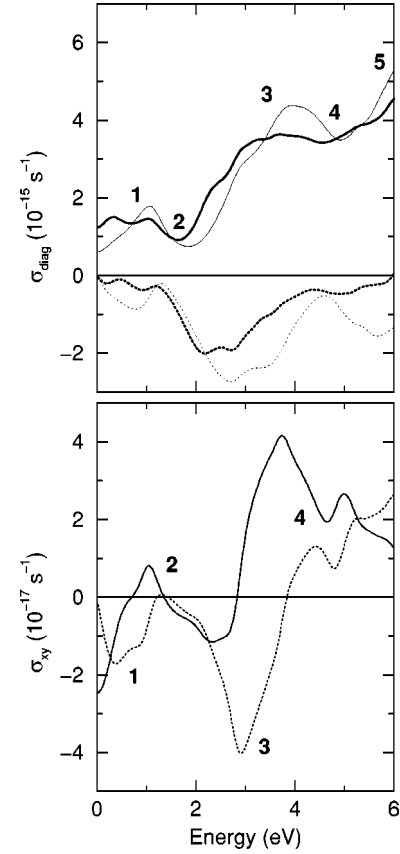


FIG. 4. Elements of the conductivity tensor for the (001) orientation of magnetization ($M||a$). The real parts of the conductivity elements are given by the solid lines and the imaginary parts by the dashed lines. In the upper panel the thick lines corresponds to σ_{xx} ($E||c$), and the thin lines to σ_{yy} ($E||a$).

B. Optical conductivity

In order to simplify the analysis of the optical spectra, we mention the following observations. First, despite the mixed spin character of the eigenstates (due to the spin-orbit coupling) the spectra of the diagonal as well as off-diagonal elements of the conductivity tensor can to a very good approximation be written as the sum of majority- and minority-spin contributions. Second, the σ_{xx} and σ_{yy} spectra show the same general features and we will restrict ourselves to discuss only those. Third, only transitions from O-*p* to Cr-*d* derived states are possible in the minority-spin channel, whereas in the majority-spin channel in addition transitions between Cr-*d* derived states can contribute.

In Fig. 4 the calculated conductivity spectra are shown. The spectra were convoluted with a Lorentzian having a half-width at half maximum $\delta=0.2$ eV to approximate finite lifetime effects. Prominent spectral features in the conductivity spectra have been labeled “1” to “5.” In order to analyze the origin of the spectral features we calculated the contributions of individual final and initial states according to their local site symmetry. As an example, we show in Fig. 5 the contributions of the final Cr-*d* states to the diagonal absorptive part (i.e., $\text{Re}[\sigma_{yy}]$), which are the most important ones for the interpretation of the spectra. The double peak 1 in

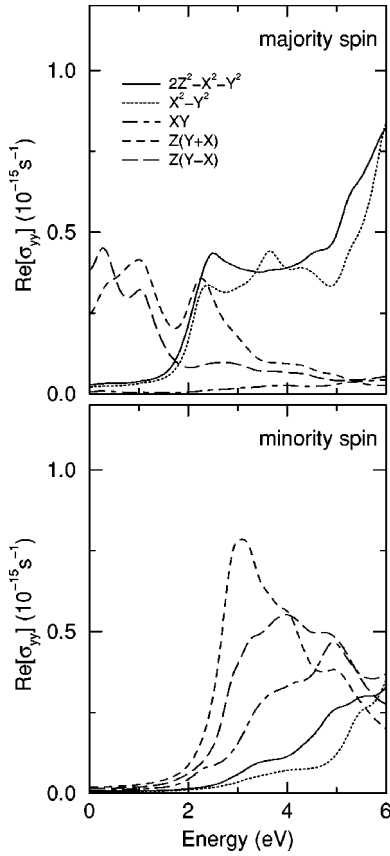


FIG. 5. The contributions of transitions to unoccupied Cr- d states to $\text{Re}[\sigma_{yy}]$ ($E||a$). The upper panel shows the contributions of the majority-spin channel, the lower panel those of the minority-spin channel.

Fig. 4 originates from Cr- $d(t_{2g})$ to Cr- $d(t_{2g})$ transitions within the majority-spin channel, which are enabled by the p - d hybridization. The minimum 2 at 1.7 eV originates from the e_g - t_{2g} gap in the majority-spin channel. The spectral increase up to shoulder 3 results from the Cr- $d(t_{2g})$ to Cr- $d(e_g)$ transitions in the majority-spin channel and the onset of O- p to Cr- $d(t_{2g})$ transitions in the minority-spin channel. Going from 3 to 4 in the majority-spin channel the contribution of the transitions from Cr- $d(t_{2g})$ vanishes and the main contribution comes from transitions originating from O- p , which results in a further increase that is connected with the PDOS peak at the top of the e_g bands. This feature is supported also by the onset of O- p to Cr- $d(e_g)$ transitions in the minority-spin channel.

In Fig. 6 the contributions of the final Cr- d states to the absorptive part of the off-diagonal conductivity (i.e., $\text{Im}[\sigma_{xy}]$) are shown. We note that only transitions from or to states with nonzero orbital moment can contribute. The cubic crystal field quenches the orbital moment in the e_g states. Therefore only transitions involving the t_{2g} states contribute significantly as only those states carry a considerable orbital moment. A similar analysis as performed for the diagonal conductivity leads to the conclusion that transitions from Cr- $d(t_{2g})$ to Cr- $d(t_{2g})$, and to Cr- $d(e_g)$, within the majority-spin channel, are responsible for the structures below 1 eV

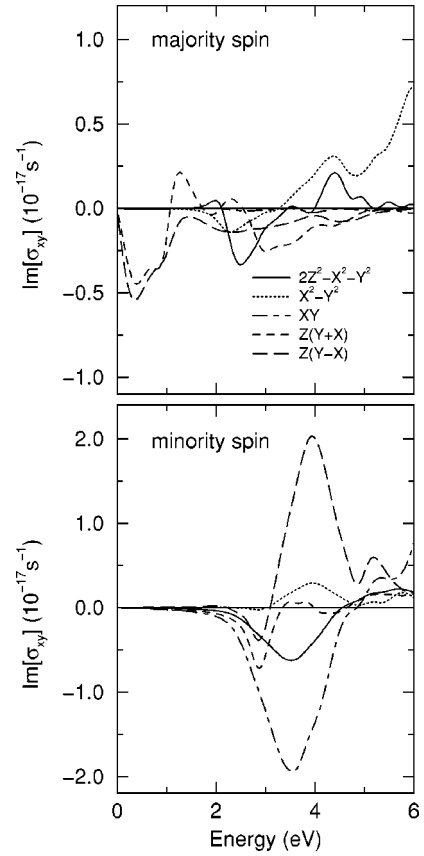


FIG. 6. The contributions of transitions to unoccupied Cr- d states to $\text{Im}[\sigma_{xy}]$. The upper panel shows the contributions of the majority-spin channel, the lower panel those of the minority-spin channel.

and above 2 eV, respectively. In the minority-spin channel only transitions from O- p to Cr- $d(t_{2g})$ states contribute significantly forming the major part of the off-diagonal conductivity above 2 eV.

C. Polar Kerr effect

In Fig. 7 the polar Kerr rotations and ellipticities calculated with the LSDA, GGA, and LSDA+ U functionals are depicted. All spectra were computed with a lifetime broadening of $\delta=0.1$ eV. The Kerr spectra were calculated using Eq. (3) for the (001) orientation of the magnetization (i.e., $M||a$). From these three theoretical results the GGA calculation achieves the best agreement with the experimental data, as can be clearly recognized from Fig. 8. All the theoretical Kerr rotation spectra exhibit a similar shape with one local minimum and one local maximum between 1 and 3 eV, while such a structure is repeated twice in the experiment. The LSDA calculation reproduces well the peaks at 1 eV and 1.5 eV, while the shoulder observed at 3.8 eV is shifted towards lower energies in the calculation. Application of the LSDA+ U leads to a more or less rigid shift of the LSDA spectrum towards higher energy, which stems from the increased gap in the minority-spin channel. The position of the shoulder at 3.8 eV is well reproduced as well as the peak at 2.4 eV. On the other hand, the agreement at lower energies is

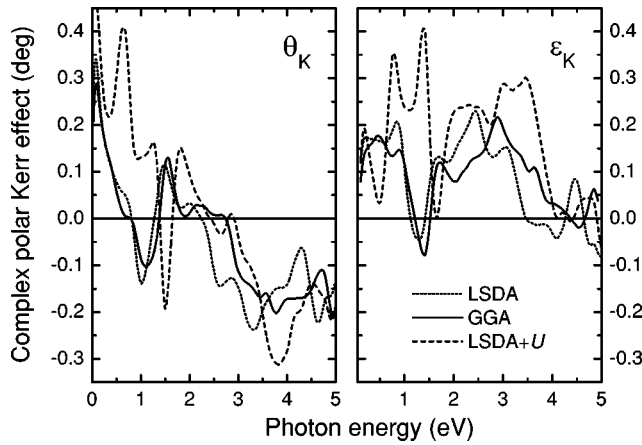


FIG. 7. The polar Kerr rotation and Kerr ellipticity of a -axis-oriented CrO_2 as calculated with LSDA, GGA, and LSDA+ U exchange-correlation functionals.

not good and the main discrepancy, which is the missing four peak structure between 1 and 3 eV, is not removed. In this respect the LSDA+ U can hardly be considered as an improvement over the LSDA. The GGA spectrum seems to combine the good features of the other two calculated spectra, see Fig. 8. As it follows the LSDA rotation spectrum up to 2 eV, it reproduces well the peaks at 1.2 and 1.5 eV. Above 3 eV it coincides with the LSDA+ U spectrum reproducing well the crossover at 2.8 eV and the shoulder at 3.8 eV. In the spectral range between 2 and 3 eV there is a sign of a local minimum at 2 eV and maximum at 2.3 eV, however, the magnitude of these features is much too small compared to the experiment. Similar conclusions can be drawn for the Kerr ellipticity. The measured Kerr ellipticity is well described by the GGA ellipticity spectrum, except for the observed minimum in the ellipticity at 2.3 eV, which is not as deep in the GGA calculated spectrum.

In the past the occurrence of a large Kerr effect in the ternary compound PtMnSb has been related to the half-metallic nature of PtMnSb.³⁸ This left the impression that large Kerr effects could be anticipated for half-metallic fer-

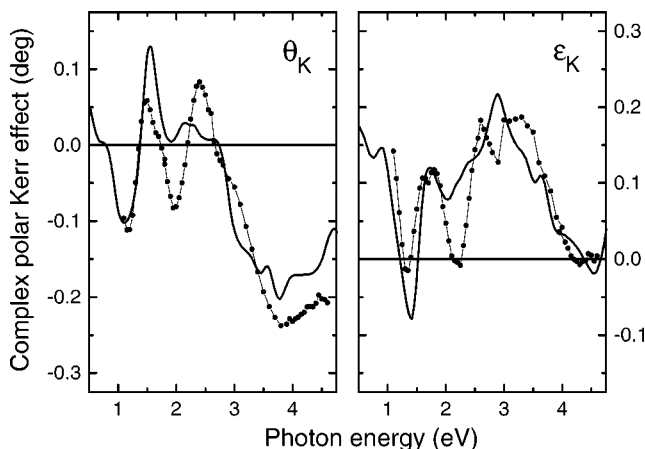


FIG. 8. Comparison of the measured, low-temperature polar Kerr spectra (symbols) and the theoretical spectra computed with the GGA approach (for a lifetime broadening $\delta=0.1$ eV).

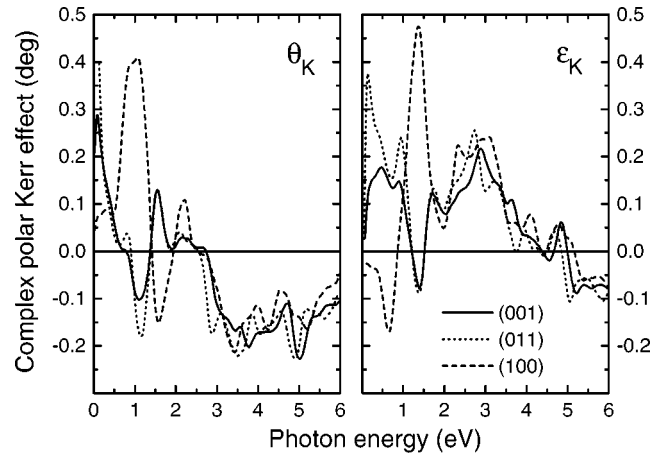


FIG. 9. The polar Kerr rotation and ellipticity spectra as calculated with the GGA functional for various orientations of the magnetization.

romagnets, yet the Kerr effect of CrO_2 is quite small, even smaller than, e.g., that of Fe. Detailed *ab initio* investigations showed that there does not exist a general rule for obtaining a large Kerr effect in a half-metallic material (see, e.g., Ref. 39). Although the half-metallic property may enhance the Kerr effect through a plasma minimum in the reflectivity, the more pronounced influence comes from the size of the spin-orbit coupling.³⁹ The strong spin-orbit coupling of Pt contributes significantly to the large Kerr effect of PtMnSb. The spin-orbit coupling of Cr as well as of O is much smaller, so that consequently only a small Kerr effect results for CrO_2 .

In Fig. 9 we show the anisotropy of the polar Kerr effect as obtained with the GGA. A large difference is present in the Kerr spectra computed for the (100) and (001) magnetization orientation below 2 eV, where the signs of the Kerr rotations are opposite, while almost the same spectrum is obtained above 3 eV. The anisotropy within the basal plane is found to be rather small. This suggests that even the orientation of crystallites with the a axis out of the plane of the film [i.e., $(0mn)$ orientation] cannot explain the remaining disagreement between the calculation and experiment. The anisotropy in the magneto-optical spectra was previously related to the magnetocrystalline anisotropy and the anisotropy in the orbital moment.^{40,41} The magnetocrystalline anisotropy in the spin and orbital moments is computed to be quite small. The orientational anisotropy of the orbital moment, $\Delta M_L = M_L[M||a] - M_L[M||c]$, is only $-0.001\mu_B$ per Cr atom, whereas the anisotropy in the Cr spin moment is practically zero. This finding is supported by another, non-full-potential investigation,³⁹ which obtained nearly identical values. The non-full-potential calculation of Ref. 20, however, predicted a much larger orbital moment anisotropy of $-0.022\mu_B$. The fact that the anisotropy in the Kerr effect in Fig. 9 is large, in spite of the very small anisotropy in the orbital moment, can be understood from the fact that the anisotropy in the orbital moment is given by a spectral integral over the anisotropy in the absorptive part of the off-diagonal conductivity.⁴¹ While at a fixed frequency the an-

isotropy in the off-diagonal spectrum may be large, the frequency-integrated anisotropy can nevertheless be small.

Finally, we studied how the absorptive (imaginary) and refractive (real) parts of the off-diagonal conductivity contribute to the Kerr spectra. Since the variables in Eq. (3) are complex, both the absorptive and refractive parts of the conductivity contribute to the rotation and ellipticity. Nevertheless, upon separating the contributions of the real and imaginary parts of the off-diagonal conductivity we found that except for the interval between 2 and 3 eV the shape of the Kerr rotation spectra is determined by the refractive part of the off-diagonal conductivity. The same holds for the Kerr ellipticity and the absorptive part of the off-diagonal conductivity. This means that the ellipticity spectrum can be understood in terms of the analysis in the previous section, while the rotation follows from it by a Kramers-Kronig transformation.

VI. CONCLUSIONS

We have measured the magneto-optical Kerr spectra on *a*-axis textured CrO₂ films. The Kerr spectra measured at low temperatures differ significantly from those obtained at 300 K. The measured Kerr spectra are compared to Kerr spectra that we calculated using the LSDA, GGA, and LSDA+*U* exchange-correlation functionals. We found satisfactory agreement between the experimental spectra and theoretical spectra calculated with the GGA functional in the spectral range from 0.5 to 5 eV, with the exception of the interval from 1.8 to 2.8 eV. The main outcome of this study is the fact that application of the LSDA+*U* scheme, which changes notably the LSDA spectra, does not result in better agreement with the experiment. Moreover, the correspondence of the LSDA+*U* spectra to the experimental ones is significantly worse than that of the GGA spectra. This shows that the LSDA+*U* functional is not adequate for the explanation of the magneto-optical properties of CrO₂, and consequently, also not adequate for appropriately describing its electronic structure.

ACKNOWLEDGMENTS

We gratefully acknowledge financial support from the Sonderforschungsbereich 463, Dresden, Germany. Parts of this work are supported by the German Federal Ministry of Education and Research ‘‘BMBF’’ under Grant No. 13N7329.

APPENDIX

The derivation of expressions for the polar Kerr rotation and ellipticity in biaxial crystals for an arbitrary direction of the linear polarization is presented here. We assume that the magnetization as well as the light *k* vector point along the *z* axis. The polarization analysis then reduces to a two dimensional problem in the *x*-*y* plane. The relevant part of the permittivity tensor reads

$$\boldsymbol{\epsilon} = \begin{pmatrix} \epsilon_{xx} & \epsilon_{xy} \\ -\epsilon_{xy} & \epsilon_{yy} \end{pmatrix}. \quad (\text{A1})$$

We adopt the notation $\Delta = \epsilon_{yy} - \epsilon_{xx}$ and $\tau = \epsilon_{xy}/\Delta$. In the following we assume τ to be a small parameter, which is well satisfied in CrO₂, where $|\tau| < 1/10$. We therefore perform the expansion only to the lowest order in τ . The eigenmodes, which are the solutions of the Fresnel equation, are to lowest order in τ given by

$$\begin{aligned} n_1 &= \sqrt{\epsilon_{xx}} + \mathcal{O}(\tau^2), & \boldsymbol{\eta}_1 &= \begin{pmatrix} 1 \\ \tau \end{pmatrix} + \mathcal{O}(\tau^2), \\ n_2 &= \sqrt{\epsilon_{yy}} + \mathcal{O}(\tau^2), & \boldsymbol{\eta}_2 &= \begin{pmatrix} \tau \\ 1 \end{pmatrix} + \mathcal{O}(\tau^2), \end{aligned} \quad (\text{A2})$$

where $n_{1,2}$ are the refractive indices and $\boldsymbol{\eta}_{1,2}$ the electric-field eigenvectors. The corresponding reflection coefficients shall be denoted $r_{1,2}$. The incident light is assumed to have a polarization vector at an angle ϕ with respect to the *y* axis,

$$\mathbf{E}^i = E_0 \begin{pmatrix} \cos \phi \\ \sin \phi \end{pmatrix} \equiv E_0 \begin{pmatrix} c \\ s \end{pmatrix}, \quad (\text{A3})$$

in which we introduce a shorthand notation for the trigonometric functions. Expressing the incoming linearly polarized light in the $\boldsymbol{\eta}_{1,2}$ basis and keeping only the terms to lowest order in τ we arrive at the following expression for the reflected light:

$$\mathbf{E}^r \propto r_1(c - s\tau)\boldsymbol{\eta}_1 + r_2(s - c\tau)\boldsymbol{\eta}_2 + \mathcal{O}(\tau^2). \quad (\text{A4})$$

Since we are not interested in the absolute intensity of the reflected light we omit the multiplicative factors. In order to derive the Kerr rotation and ellipticity we express the above equation in the basis of circular polarizations.

The choice of the circular polarization basis is not unique (there is an arbitrary phase shift between the two polarizations). The choice of this phase shift is related to the direction from which we measure the rotation of the polarization plane. Since we would like to use the fact that the angle between the polarization planes of the incident and reflected light is small, we have to choose the above-mentioned phase shift so that the rotation of the polarization plane of the incident light is zero. This could be done in two steps: first we express $\boldsymbol{\eta}_1, \boldsymbol{\eta}_2$ in the rotated coordinate system whose *x* axis is along the polarization plane of the incident light, and, second, transform these ‘‘new’’ vectors into the circular basis $(1, i), (1, -i)$. We arrive at the following representation of the basis vectors:

$$\begin{aligned} \boldsymbol{\eta}_1 &= \begin{pmatrix} c(1 - i\tau) + s(\tau + i) \\ c(1 + i\tau) + s(\tau - i) \end{pmatrix}, \\ \boldsymbol{\eta}_2 &= \begin{pmatrix} c(\tau - i) + s(1 + i\tau) \\ c(\tau + i) + s(1 - i\tau) \end{pmatrix}. \end{aligned} \quad (\text{A5})$$

Substitution into Eq. (A4) yields

$$E^r \propto r_1 \begin{pmatrix} ce^{i\phi} - i\tau \\ ce^{-i\phi} + i\tau \end{pmatrix} + r_2 \begin{pmatrix} -ise^{i\phi} + i\tau \\ ise^{-i\phi} - i\tau \end{pmatrix} + \mathcal{O}(\tau^2). \quad (\text{A6})$$

We are obviously interested only in the magnetic part of the rotation and ellipticity. This part can be obtained by measuring the rotation and ellipticity for the two antiparallel orientations of the magnetic field and subtracting the two results, i.e.,

$$\Theta_K = \frac{1}{2}[\Theta_K(+M) - \Theta_K(-M)], \quad (\text{A7})$$

where we denote $\Theta_K \equiv \theta_K + i\epsilon_K$. For small Θ_K we can use the approximation

$$e^{2i\Theta_K} \approx \frac{E_+^r}{E_-^r}. \quad (\text{A8})$$

Starting from this approximation we arrive at

$$e^{4i\Theta_K} \approx 1 + 4i\Theta_K \approx \frac{E_+^r(+M) E_-^r(-M)}{E_-^r(+M) E_+^r(-M)} \equiv \frac{N}{D},$$

$$4i\Theta_K \approx \frac{N-D}{D}. \quad (\text{A9})$$

Using Eq. (A6), and that $\tau \rightarrow -\tau$ for $M \rightarrow -M$, we obtain

$$N = E_-^r(+M)E_+^r(-M) = r_1^2 c^2 + r_2^2 s^2 + 2i\tau\{-r_1^2 c^2 + r_2^2 s^2 + r_1 r_2(c^2 - s^2)\} + \mathcal{O}(\tau^2), \quad (\text{A10})$$

$$D = E_+^r(+M)E_-^r(-M) = r_1^2 c^2 + r_2^2 s^2 + 2i\tau\{r_1^2 c^2 - r_2^2 s^2 - r_1 r_2(c^2 - s^2)\} + \mathcal{O}(\tau^2). \quad (\text{A11})$$

Substituting into Eq. (A9) and keeping only the lowest-order term in τ we find

$$\Theta_K = -\tau \frac{r_1^2 c^2 - r_2^2 s^2 - r_1 r_2(c^2 - s^2)}{r_1^2 c^2 + r_2^2 s^2}$$

$$= \epsilon_{xy} \left(\frac{r_2 - r_1}{\epsilon_{yy} - \epsilon_{xx}} \right) \frac{r_1 \cos^2 \phi + r_2 \sin^2 \phi}{r_1^2 \cos^2 \phi + r_2^2 \sin^2 \phi}. \quad (\text{A12})$$

The reflection coefficients r_i are given by the standard expression for normal incidence,

$$r_i = \frac{n_i - n_0}{n_i + n_0}. \quad (\text{A13})$$

If we assume random orientation of crystallites with respect to the polarization of the incoming light, the Kerr rotation and ellipticity are obtained by averaging Eq. (A12) over the angle ϕ , which yields

$$\theta_K + i\epsilon_K \approx \frac{2\epsilon_{xy}}{\epsilon_{yy} - \epsilon_{xx}} \frac{r_y - r_x}{r_y + r_x}. \quad (\text{A14})$$

We emphasize that the above derivation is based on the assumption that the optical birefringence, introduced by the difference of the diagonal elements, is much larger than the magneto-optical effect described by the off-diagonal element. This assumption does not mean that the nonmagnetic rotation and ellipticity are larger than the magnetic contribution. The magnetic effect is more or less independent of the angle ϕ , while the nonmagnetic effect is largest for $\phi = \pi/4$ and zero for $\phi = 0, \pi/2$. The standard expression for the polar Kerr effect corresponds to the other limit than the one we describe here, i.e., $\Delta \ll \epsilon_{xy}$. In the latter limit case, we would obtain^{42,43}

$$\theta_K + i\epsilon_K \approx \frac{-\epsilon_{xy}}{(1 - \epsilon_a)\epsilon_a^{1/2}} + \mathcal{O}\left(\frac{\Delta}{\epsilon_{xy}}\right)^2, \quad (\text{A15})$$

where $\epsilon_a \equiv (\epsilon_{xx} + \epsilon_{yy})/2$.

¹K. Schwarz, J. Phys. F: Met. Phys. **16**, L211 (1986).

²K. P. Kämper, W. Schmitt, G. Güntherodt, R. J. Gambino, and R. Ruf, Phys. Rev. Lett. **59**, 2788 (1987).

³R. Wiesendanger, H.-J. Güntherodt, G. Güntherodt, R. J. Gambino, and R. Ruf, Phys. Rev. Lett. **65**, 247 (1990).

⁴H. Y. Hwang and S.-W. Cheong, Science **278**, 1607 (1997).

⁵R. J. Soulen, J. M. Byers, M. S. Osofsky, B. Nadgorny, T. Ambrose, S. F. Cheng, P. R. Broussard, C. T. Tanaka, J. Nowak, J. S. Moodera, A. Barry, and J. M. D. Coey, Science **282**, 85 (1998).

⁶X. W. Li, A. Gupta, and G. Xiao, Appl. Phys. Lett. **75**, 713 (1999).

⁷C. B. Stagarescu, X. Su, D. E. Eastman, K. N. Altmann, F. J. Himpsel, and A. Gupta, Phys. Rev. B **61**, R9233 (2000).

⁸F. Y. Fang, C. L. Chien, E. F. Ferrari, X. W. Li, G. Xiao, and A. Gupta, Appl. Phys. Lett. **77**, 286 (2000).

⁹Y. Ji, G. J. Strijkers, F. Y. Yang, C. L. Chien, J. M. Byers, A. Anguelouch, G. Xiao, and A. Gupta, Phys. Rev. Lett. **86**, 5585 (2001).

¹⁰J. S. Moodera, L. R. Kinder, T. M. Wong, and R. Meservey, Phys. Rev. Lett. **74**, 3273 (1995).

¹¹A. Gupta, X. W. Li, and G. Xiao, Appl. Phys. Lett. **78**, 1894 (2001).

¹²H. Y. Hwang, S.-W. Cheong, N. P. Ong, and B. Batlogg, Phys. Rev. Lett. **77**, 2041 (1996).

¹³S. S. Manoharan, D. Elefant, G. Reiss, and J. B. Goodenough, Appl. Phys. Lett. **72**, 984 (1998).

¹⁴J. M. D. Coey, A. E. Berkowitz, L. Balcells, F. F. Putris, and A. Barry, Phys. Rev. Lett. **80**, 3815 (1998).

¹⁵V. I. Anisimov, J. Zaanen, and O. K. Andersen, Phys. Rev. B **44**, 943 (1991).

¹⁶V. I. Anisimov, I. V. Solovyev, M. A. Korotin, M. T. Czyzyk, and G. A. Sawatzky, Phys. Rev. B **48**, 16 929 (1993).

¹⁷M. A. Korotin, V. I. Anisimov, D. I. Khomskii, and G. A. Sawatzky, Phys. Rev. Lett. **80**, 4305 (1998).

¹⁸I. I. Mazin, D. J. Singh, and C. Ambrosch-Draxl, Phys. Rev. B **59**, 411 (1999).

¹⁹H. Brändle, D. Weller, J. C. Scott, J. Sticht, P. M. Oppeneer, and G. Güntherodt, in *Physics of Transition Metals*, edited by P. M. Oppeneer and J. Kübler (World Scientific, Singapore, 1993), p. 345.

- ²⁰Y. A. Uspenskii, E. T. Kulatov, and S. V. Halilov, *Phys. Rev. B* **54**, 474 (1996).
- ²¹S. Ishibashi, T. Namikawa, and M. Satou, *Mater. Res. Bull.* **14**, 51 (1979).
- ²²B. L. Chamberland, *Crit. Rev. Solid State Mater. Sci.* **7**, 1 (1977).
- ²³U. Rüdiger, C. König, M. Rabe, S. Senz, and G. Güntherodt (unpublished).
- ²⁴J. S. Kouvel and D. S. Rodbell, *J. Appl. Phys.* **38**, 979 (1967).
- ²⁵H. Brändle, D. Weller, S. S. P. Parkin, J. C. Scott, P. Fumagalli, W. Reim, R. J. Gambino, R. Ruf, and G. Güntherodt, *Phys. Rev. B* **46**, 13 889 (1992).
- ²⁶P. Blaha, K. Schwarz, and J. Luitz, computer code WIEN97 (Technische Universität Wien, Vienna, 1999).
- ²⁷J. Kuneš, P. Novák, M. Diviš, and P. M. Oppeneer, *Phys. Rev. B* **63**, 205111 (2001).
- ²⁸J. Kuneš and P. Novák, *J. Phys.: Condens. Matter* **11**, 6301 (1999).
- ²⁹P. M. Oppeneer, T. Maurer, J. Sticht, and J. Kübler, *Phys. Rev. B* **45**, 10 924 (1992).
- ³⁰J. P. Perdew and Y. Wang, *Phys. Rev. B* **45**, 13 244 (1992).
- ³¹J. P. Perdew, K. Burke, and M. Ernzerhof, *Phys. Rev. Lett.* **77**, 3865 (1996).
- ³²P. Novák, F. Boucher, P. Gressier, P. Blaha, and K. Schwarz, *Phys. Rev. B* **63**, 235114 (2001).
- ³³A. I. Liechtenstein, V. I. Anisimov, and J. Zaanen, *Phys. Rev. B* **52**, R5467 (1995).
- ³⁴S. Matar, G. Demazeau, J. Sticht, V. Eyert, and J. Kübler, *J. Phys. I* **2**, 315 (1992).
- ³⁵P. I. Sorantin and K. Schwarz, *Inorg. Chem.* **31**, 567 (1992).
- ³⁶S. P. Lewis, P. B. Allen, and T. Sasaki, *Phys. Rev. B* **55**, 10 253 (1997).
- ³⁷N. E. Brener, J. M. Tyler, J. Callaway, D. Bagayoko, and G. L. Zhao, *Phys. Rev. B* **61**, 16 582 (2000).
- ³⁸R. A. de Groot, F. M. Mueller, P. G. van Engen, and K. H. J. Buschow, *J. Appl. Phys.* **55**, 2151 (1984).
- ³⁹P. M. Oppeneer, in *Handbook of Magnetic Materials*, edited by K. H. J. Buschow (Elsevier, Amsterdam, 2001), Vol. 13, pp. 229–422.
- ⁴⁰D. Weller, G. R. Harp, R. F. C. Farrow, A. Cebollada, and J. Sticht, *Phys. Rev. Lett.* **72**, 2097 (1994).
- ⁴¹P. M. Oppeneer, *J. Magn. Magn. Mater.* **188**, 275 (1998); J. Kuneš and P. M. Oppeneer, *Phys. Rev. B* **61**, 15 774 (2000).
- ⁴²P. Fumagalli, Ph.D. thesis, Eigenossische Technische Hochschule Zürich, 1990.
- ⁴³P. M. Oppeneer, I. Galanakis, P. James, O. Eriksson, and P. Ravindran, *J. Magn. Soc. Jpn.* **23**, S1, 21 (1999).